remote sensing

MDPI

Article

A Comparative Analysis of the Effect of Orbital Geometry and Signal Frequency on the Ionospheric Scintillations over a Low Latitude Indian Station: First Results from the 25th Solar Cycle

Ramkumar Vankadara [1], Nirvikar Dashora [2], Sampad Kumar Panda [1,*] and Jyothi Ravi Kiran Kumar Dabbakuti [3]

[1] Department of ECE, KL Deemed to be University, Koneru Lakshmaiah Education Foundation, Guntur 522302, Andhra Pradesh, India; 2002040005@kluniversity.in
[2] National Atmospheric Research Laboratory, Gadanki 517112, Andhra Pradesh, India; ndashora@narl.gov.in
[3] Department of Internet of Things, KL Deemed to be University, Koneru Lakshmaiah Education Foundation, Guntur 522302, Andhra Pradesh, India; d.kirankumar@kluniversity.in
* Correspondence: sampadpanda@kluniversity.in or sampadpanda@gmail.com; Tel.: +91-9392665582

Abstract: The equatorial post-sunset ionospheric irregularities induce rapid fluctuations in the phase and amplitude of global navigation satellite system (GNSS) signals which may lead to the loss of lock and can potentially degrade the position accuracy. This study presents a new analysis of L-band scintillation from a low latitude station at Guntur (Geographic 16.44°N, 80.62°E, dip 22.18°), India, for the period of 18 months from August 2021 to January 2023. The observations are categorized either in the medium Earth-orbiting (MEO) or geosynchronous orbiting (GSO) satellites (GSO is considered as a set of the geostationary and inclined geosynchronous satellites) for L1, L2, and L5 signals. The results show a higher occurrence of moderate ($0.5 < S4 \leq 0.8$) and strong ($S4 > 0.8$) scintillations on different signals from the MEO compared to the GSO satellites. Statistically, the average of peak S4 values provides a higher confidence in the severity of scintillations on a given night, which is found to be in-line with the scintillation occurrences. The percentage occurrence of scintillation-affected satellites is found to be higher on L1 compared to other signals, wherein a contrasting higher percentage of affected satellites over GSO than MEO is observed. While a clear demarcation between the L2/L5 signals and L1 is found over the MEO, in the case of GSO, the CCDF over L5 is found to match mostly with the L1 signal. This could possibly originate from the space diversity gain effect known to impact the closely spaced geostationary satellite links. Another major difference of higher slopes and less scatter of S4 values corresponding to L1 versus L2/L5 from the GSO satellite is found compared to mostly non-linear highly scattered relations from the MEO. The distribution of the percentage of scintillation-affected satellites on L1 shows a close match between MEO and GSO in a total number of minutes up to ~60%. However, such a number of minutes corresponding to higher than 60% is found to be larger for GSO. Thus, the results indicate the possibility of homogeneous spatial patterns in a scintillation distribution over a low latitude site, which could originate from the closely spaced GSO links and highlight the role of the number of available satellites with the geometry of the links, being the deciding factors. This helps the ionospheric community to develop inter-GNSS (MEO and GSO) operability models for achieving highly accurate positioning solutions during adverse ionospheric weather conditions.

Keywords: ionosphere; amplitude scintillation; multi-frequency GNSS; multi-constellation; satellite geometry

Citation: Vankadara, R.; Dashora, N.; Panda, S.K.; Dabbakuti, J.R.K.K. A Comparative Analysis of the Effect of Orbital Geometry and Signal Frequency on the Ionospheric Scintillations over a Low Latitude Indian Station: First Results from the 25th Solar Cycle. *Remote Sens.* **2024**, *16*, 1698. https://doi.org/10.3390/rs16101698

Academic Editors: Roberta Tozzi, Giuseppe Consolini and Tommaso Alberti

Received: 12 March 2024
Revised: 5 May 2024
Accepted: 7 May 2024
Published: 10 May 2024

1. Introduction

The ionospheric plasma density irregularities associated with the equatorial plasma bubbles impose sudden variations in the amplitude and phase of the signal received from satellite to receiver that are termed ionospheric scintillations [1]. Scintillations can lead to the loss of lock (LoL) which may affect the performance of positioning algorithms in

a receiver, directly impeding the accuracy and the validation of the solution [2–6]. The radio signals from the satellite to the receiver are subject to various other effects that include orbit errors, clock errors at the satellite and receiver, ionospheric and tropospheric delays, multipath, and noise. Global navigation satellite system (GNSS) signals are used in all modes of transportation, including space platforms, aircraft, marine, train, road, and public transportation, and support a large number of applications which demand precise timing and positioning solutions. Position, navigation, and timing (PNT) play a crucial part in telecoms, land mapping, law enforcement, emergency reaction, precision gardening, mining, banking, and scientific research. The standalone single-frequency measurements cannot give more accurate position values; however, with support from multi-constellation and multi-frequency observations, better position accuracies can be achieved [7]. Although there have been progressive improvements in understanding, modeling, and mitigation of various error sources in GNSS-PNT solutions, the spatiotemporal characteristics of ionospheric scintillation over any region are not yet fully understood due to the complex origin and the dynamics of the ionospheric irregularities and sparse availability of monitoring techniques.

The scintillation measurements can be acquired by ground-based single or multi-constellation and multi-frequency GNSS scintillation monitoring receivers. From the vast literature on ionospheric scintillations, it is well known that the equatorial and low latitude scintillations show a prominent solar activity, season and local time dependence [8,9]. In this scenario, different constellations have different frequencies and chipping rates that contribute to varying robustness against signal scintillation [10,11] and hence translate into a dominant solar activity, season, and local time-dependent effects on kinematic precise point positioning [3]. A greater number of constellations provides a greater number of visible satellites and hence more ionospheric pierce points (IPPs) above a given GNSS station. Many previous studies around the globe have used multi-constellation data to analyze the spatiotemporal variations in the equatorial and low-latitude ionosphere. Sales et al. [12,13] have performed an extensive review of the equatorial and low latitude scintillation and fading on three GPS signals at L1, L2, and L5 in the South American sector. Previous studies, for example, the one by Moraes et al. [14], have shown the scintillation effects at the GPS L1 for a period of 32 days during the high solar activity period under the solar cycle 23. Their results confirmed the reports from previous studies showing an increase in S4 related to enhanced fading which implies a higher probability of the loss of lock. Guo et al. [15] presented the temporal and spatial features of the ionospheric scintillation at GPS L1 at five different monitoring stations during 2011–2015, wherein the scintillation is seen to be exhibiting a strong seasonal pattern with varying occurrence rates and amplitude scintillation probabilities of different intensities. Jiao et al. [16] used observations at three signals including GPS L1, L2C, and L5 to provide insights into the impact of strong scintillation. Their results also emphasized the signal fading level, duration, and inter-frequency fading distribution during the scintillation events. They showed that simultaneous fading on the three signals occurs rarely, suggesting that a robust performance can be achieved by using multi-frequency signal-aiding techniques. Similar findings are obtained by Delay et al. [17] and Carrano et al. [18] stating that the signal tracking at L2C and L5 is less robust to scintillation effects than at the legacy L1 signal. The statistical characterization of GPS triple frequency scintillation is presented by Moraes et al. [19], showing a higher probability for intense scintillation at the L5 and L2C compared to L1. In another study, they have extended results to show that L5 has the highest probability of fades < -10 dB when compared to L2 and L1 [20]. The L-band amplitude scintillations over the Dakar station (Africa) were studied by Akala et al. [21] who found the post-sunset scintillation occurrence with the highest daily scintillations recorded between 22:00–02:00 LT. Similarly, Ghafoori and Skone [22] investigated the impact of L-band scintillation on GPS receivers using several real and synthetic data sets from the equatorial region stations, collected between June 2012 to March 2013. This led to the development of realistic simulation tools and the evaluation of GNSS signals as well as receiver performance in Rio

de Janeiro. Similarly, the S4 values were analyzed for the local nighttime at Kototabang, Indonesia, from February 2006 to November 2007 by Otsuka et al. [23] who reported a high scintillation occurrence rate between 20:00 and 01:00 LT. Most of the results from equatorial scintillations show the presence of total electron content (TEC) depletions accompanied by scintillation occurrences [24,25]. The EPBs are the large plasma density depletion regions formed through nonlinear Rayleigh–Taylor instability in the post-sunset period [26]. Theoretically, the diffraction and the radio wave scattering processes inside a growing EPB manifest scintillation effects on the traversing radio signals [27,28]. The relationship between the EPBs and the L-band scintillations has been advanced through some of the major observational as well as theoretical studies such as Kelley et al. [29], Ledvina and Makela [30], Carrano et al. [31], and Bhattacharyya et al. [32]. These studies (and references therein) have emphasized the roles of signal propagation direction, its alignment with the field-aligned EPBs and the severity of scintillations across the spectrum of the observed ionospheric irregularities over the equatorial and low latitude regions.

As far as the Indian ionospheric region is concerned, it is strongly influenced by the presence of the geomagnetic equator passing right through the southernmost tip of the Indian peninsular region. Thus, the navigation solution in and around the complete Indian landmass is prone to scintillation threats. The signal-to-noise ratio (SNR) from the L1 signals of the GPS and GLONASS recorded at Calcutta, an anomaly crest location in the Indian sector, during the high solar active years (1999–2002) had shown simultaneous scintillation effects on multiple satellite links during the post-sunset to midnight hours [33]. Goswami et al. [34] analyzed the three GPS signals L1, L2C, and L5 at the same location revealing the existence of more decorrelation among the three signals during scintillation patches corresponding to high S4. The co-existence of scintillations at GPS L1 and TEC depletions which were found to be associated with the EPBs was reported first by Dashora and Pandey [25] from single station observations, whereas multi-station scintillation characteristics over the Indian region during 2004–2005 were presented by Ram Rao et al. [35]. Srinivasu et al. [36] were the first from the Indian region to report multi-constellation multi-frequency observations from an Indian low latitude station during 2014–2017 using the L1 signals of GPS and GLONASS with a clear solar activity dependence. Sripathi et al. [37] revealed an equinoctial asymmetry in the occurrence of plasma irregularities and scintillations for the year 2015 using three Ionosondes and three GPS receivers located in the Indian region. A correlation between the optical and L-band measurements of the ionospheric irregularities was presented by Paul et al. [38] for the low solar activity period. Earlier studies on the occurrence characteristics of the VHF and GPS scintillations at low latitude stations report intense scintillations during pre-midnight hours and relatively weaker scintillations during the post-midnight hours [39,40]. The effect of the low latitude scintillations on LoL occurrences at GPS and GLONASS signals during 2014–2017 was presented by Srinivasu et al. [2]. Their results show that the LoL occurrence is a complex function of local time, elevation angle, and the amplitude (S4)/phase (σ_{φ}) scintillation indices combination besides its varying patterns according to season and solar activity during the solar cycle 24. A similar study but with data from only one equinoctial month of solar active year 2014 was performed by Biswas and Paul [41] in terms of occurrence and duration of cycle slip and LoL at the northern anomaly crest location in India. They highlight the susceptibility of GLONASS L1 CA among all GNSS signals and the resistant characteristics of Galileo signals among the primary L1 signals from only three constellations (GPS, GLONASS, Galileo).

However, there have been no studies on the scintillation occurrence from the Indian region which cover the effect on all the transmitting frequencies of visible GNSS constellations at a low latitude location during the current solar cycle 25. The observations presented in this study are from August 2021 to January 2023 which is in the background of continuously growing solar activity after a quiescent solar minima during 2020. Further, with the increasing number of geostationary and geosynchronous (GSO) navigation satellites over the Indian region, an investigation of the scintillation effect in comparison to medium Earth-orbiting (MEO) satellites is highly required. This paper aims to present a compre-

hensive analysis of scintillation scenarios using the recorded S4 indices from all the GNSS signals with a comparison between GSO and MEO signals at a low latitude station in terms of intensity, S4 peak, occurrence rate, and the number of satellites affected with a frequency dependence approach. Section 2 describes the Materials and Methods, Section 3 shows the results, Section 4 shows the discussion, and Section 5 provides conclusions of the present study.

2. Materials and Methods

The S4 data used in this study are recorded using a multi-constellation and multi-frequency professional GNSS Ionospheric Scintillations and TEC Monitoring receiver (Septentrio make PolaRx5S receiver along with Tallysman make VeraChoke choke ring antenna/Septentrio, Belgium) at a low latitude Indian station (KLEF; Koneru Lakshmaiah Education Foundation; Geographic 16.44°N, 80.62°E) in Guntur, India. The receiver provides the data in ISMR (ionospheric scintillation monitoring record) format containing the total estimated S4 and S4 corrections for all visible constellations along with other orbital and ionospheric parameters. Scintillations are monitored for the period of 18 months from August 2021 to January 2023 which corresponds to the rising phase of the solar cycle 25.

The geometry of the different satellite-receiver links from all the constellations over the study location KLEF is verified using the IPP trajectories. It is pertinent to note here that in this part of the globe, navigation satellites with varying altitudes and orbits are visible. The available satellites are classified into medium Earth orbit (MEO) and geosynchronous orbit (GSO), wherein the satellites are in the inclined GSO (IGSO) as well as in the geostationary equatorial orbit (GEO) as shown in Figure 1. The location of IPPs from the GEO and IGSO satellites is significant to characterize the scintillations vis-a-vis the zonal drift, width, and spacing related to EPBs (Costa et al., 2020) [42] and their manifestation over low latitudes. The KLEF study location is marked with red color in all the subplots where the MEO IPP trajectories are shown in blue, IGSO in green, and GEO in magenta colors as provided in the legend.

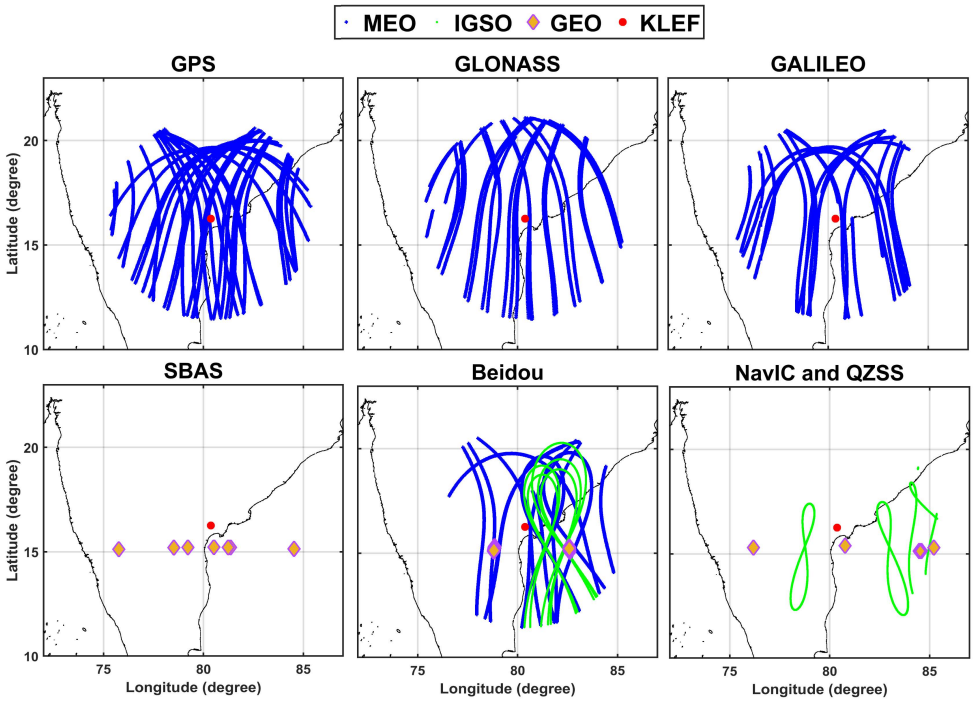

Figure 1. The IPP trajectory of satellite links for all the available constellations at the study location (KLEF) on 27 August 2022. The location of the GNSS station is marked with a red color dot, whereas the IPP trajectories of MEO, IGSO, and GEO satellites under all constellations are represented by blue, green, and magenta color dots, respectively (see legend).

In this work, the S4 of MEO and GSO satellites from the GPS, GALILEO, GLONASS, QZSS, BeiDou, SBAS, and NavIC constellations are analyzed throughout the observation period (the constellations' names are abbreviated as per the international norms). The total number of signals and frequencies available under each constellation and corresponding MEO/GSO group is provided in Table 1 which is obtained from observations during October 2022.

Table 1. Different GNSS constellations and frequencies of signals used in the present study (as observed during October 2022) along with the number of PRNs transmitting the respective signals during the whole observation period.

Constellation/Group	L1 (Frequency in MHz) (Number of PRNs)	L2 (Frequency in MHz) (Number of PRNs)	L5 (Frequency in MHz) (Number of PRNs)	Mean Altitude (Km)
GPS (MEO)	L1CA: 1575.42 (32)	L2C: 1227.60 (24)	L5 (I + Q): 1176.45 (17)	~20,200
GLONASS (MEO)	L1CA: 1602 (24)	L2C: 1246 (21)		~19,100
GALILEO (MEO)	L1BC: 1575.42 (21)	E5b: 1207.14 (21)	E5a: 1176.45 (21)	~23,222
SBAS (GEO)	L1CA: 1575.42 (8)		L5: 1176.45 (6)	~36,000
QZSS (1 GEO + 3 IGSO)	L1CA: 1575.42 (6)	L2C: 1227.60 (5)	L5: 1176.45 (5)	~36,000
BeiDou (MEO + 3 GEO + 2 IGSO)	B1: 1561.098 (26)	B3: 1268.52 (26) B2: 1207.14 (13)		~21,500 (MEO) ~36,000 (GEO)
NavIC (3 GEO + 4 IGSO)	-	-	L5: 1176.45 (5)	~36,000

The amplitude scintillation is described using the *S*4 index derived for signal intensities from all the satellite links. The total *S*4 corresponding to a satellite link is estimated as the standard deviation of raw 50 Hz signal intensity to the normalized average signal intensity over 60 s [43]. The total *S*4 including the ambient noise is calculated as in Equation (1) [44].

$$S4_{total} = \sqrt{\frac{\langle SI^2 \rangle - \langle SI \rangle^2}{\langle SI \rangle^2}} \quad (1)$$

where $\langle SI \rangle$ is the average signal intensity over 60 s with 3000 samples. The *corrected S*4 removes the ambient noise from the raw data and is calculated per minute as shown in Equation (2). For simplicity, the *corrected S*4 is hereafter mentioned as the S4 index or simply S4 throughout the study.

$$Corrected\ S4 = \sqrt{S4^2_{total} - S4^2_{noise}} \quad (2)$$

In previous studies, the scintillations have been classified based on their intensities into weak ($0.17 < S4 \leq 0.3$), moderate ($0.3 < S \leq 0.45$), and strong ($S4 > 0.45$) [35,36,45] which was based on fading depth. However, some recent studies have emphasized that the severity of scintillation can be classified based on its relationship with the Loss of Lock (LoL) [2,4–6]. Hence, following Humphreys et al. [46,47], Jordi Vilà-Valls et al. [48], and Salles et al. [12,13], we have defined the scintillation into three categories of weak ($0.2 < S4 \leq 0.5$), moderate ($0.5 < S4 \leq 0.8$), and strong scintillations ($S4 > 0.8$). The nighttime scintillation analysis is considered only from the local post-sunset to pre-dawn period (17:30 to 5:30 IST which corresponds from 12:00 to 24:00 UT). A 30° elevation cut-off is also applied to minimize possible errors due to the multipath effect and ground interference [49]. To further reduce the multipath, the satellites or PRNs, whose scintillation peak consistently remains unaltered or the S4 pattern is repeated continuously for multiple days, are discarded from the analysis. The scintillation occurrence rate per season is given for MEO and GSO constellations and available frequencies. The seasonal scintillation occurrence rate is calculated as given in Equation (3).

$$Scintillation\ occurrence\ rate = \frac{number\ of\ S4\ (weak,\ moderate,\ strong)}{number\ of\ total\ S4 > 0.2} * 100 \quad (3)$$

In the above, the numerator corresponds to the number of observations whose S4 > 0.2, and the denominator resembles the total number of S4 observations during a night which is calculated as the number of minutes from all the available satellites.

The complementary cumulative distribution frequency (CCDF) for S4 occurrences on MEO and GSO satellite links is estimated following the formulation given by Sales et al. (2021) [12]. Since the observations include all the GNSS, SBAS, and NavIC satellite links for 18 months ($N_{S4} \ll N$), the following CCDF is found to provide similar confidence as given in the above cited reference.

$$CCDF = \frac{N_{S4}}{N} \tag{4}$$

where N is the total number of samples for the combination of satellites and signals throughout the observation period, and N_{S4} is the accumulated number of minutes for the complimentary S4 bin, showing the number of minutes with S4 values greater than the bin value.

Since it aims to obtain the difference in scintillation occurrences and severity, we divided the signals into two different classes based on the type of orbiting satellites, namely (i) geostationary and inclined geosynchronous satellites, both collectively referred to as GSO and (ii) medium Earth-orbiting satellites referred to as MEO in this study.

3. Results

The results provide a detailed analysis of the characteristics of the amplitude scintillation index (S4) throughout the observation period for all the available constellations and signals in terms of the intensity, peak values, occurrence rate, number of satellites affected, and scintillation distribution from a low latitude location at KLEF campus in India. As noted in the previous section, the analysis of observations is performed for two main groups of satellites, one is MEO and the second is IGSO + GEO referred to as GSO in this study.

Figure 2 is prepared to showcase the peak S4 value for each signal observed every minute from all the visible MEO and GSO satellites in the category of weak (green), moderate (blue), and strong (red) scintillations. Following the classification of Table 1, the results in this study correspond to three signals. The dark grey background in each panel of Figure 2 represents no significant scintillation values (S4 < 0.2). From Figure 2, it is inferred that strong scintillations are mostly observed in the season of the September equinox of 2022, followed by the March equinox of 2022. In the September equinox of 2021, majorly weak to moderate scintillations are observed. All three signals and MEO/GSO constellations mostly follow seasonal patterns showing strong scintillations in equinox and weak or no scintillations in solstice seasons (from June to August and December to January). It is clearly observed that strong scintillations are mostly developed after about 19 IST and continue till the pre-midnight periods. Weak scintillation activity is observed in the span of a few hours after the midnight period. Visual inspection of Figure 2 shows that the GSO satellites are found to exhibit a lesser extent of severe scintillation values than the MEO satellites at all three signals which could be originating from several effects. The first reason could be a higher number of visible satellites (or IPPs) in MEO and the second could be the zonal movement and orientation of the EPBs which could align with MEO links in the satellite–EPB–receiver geometry at a higher probability compared to GSO (Sousasantos et al., 2022) [50]. Another difference is seen in the larger occurrence of moderate scintillations at GSO-L2 and L5 (columns four and six from the left in Figure 2), compared to GSO-L1(column 2 in Figure 2). A similar difference is found between MEO-L1 and MEO-L2/L5 for the higher occurrence and extent of red color patches on later signals corresponding to strong scintillations, which is attributed to the well-known inverse relationship of the frequency of signal and impact of scintillations [1]. Overall, the scintillation activity is found to be enhanced following the growth in solar activity during the period. The seasonal occurrence as seen in the results of Figure 2 matches well with previous studies on the low latitude S4 occurrence from the MEO (GPS and GLONASS constellations)

(e.g., [21,36,51,52]). However, the results of Figure 2 are different when a comparison is performed between MEO and GSO observations. These new results reinforcing the idea of different patterns of S4 occurrence depending upon the geometry of the satellite-receiver link have possible implications for futuristic forecast models of scintillations [50,53]. This study attempts to analyze such implications through a detailed investigation of each of these patterns.

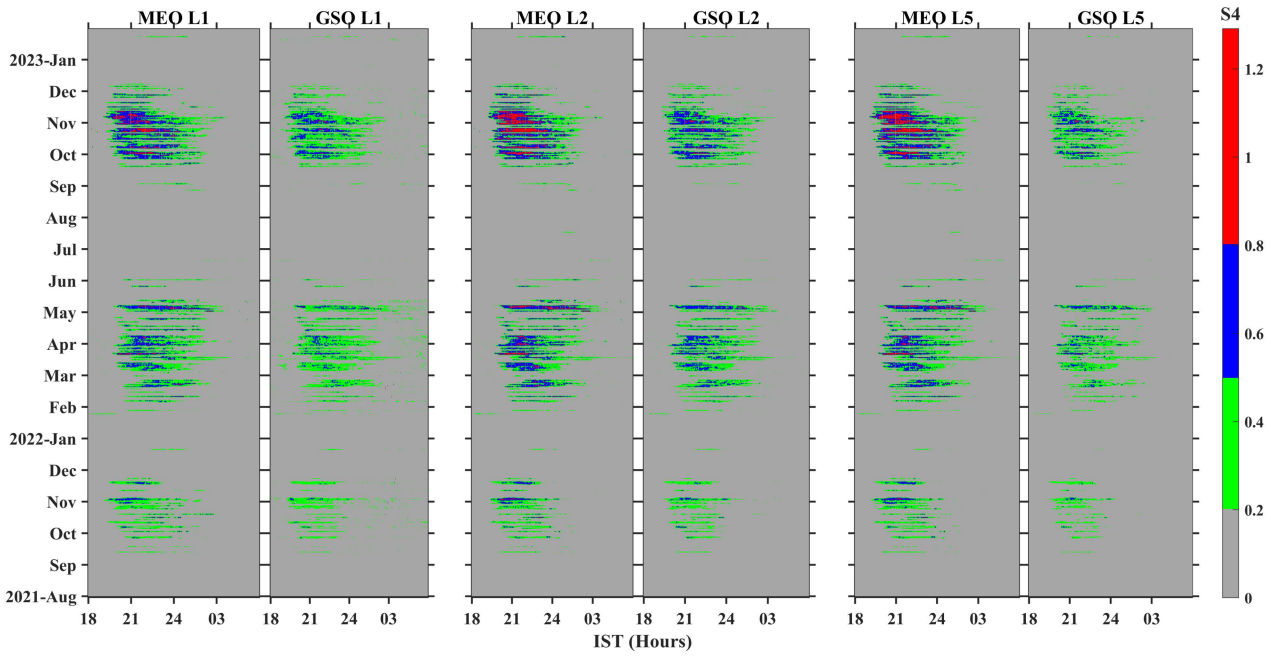

Figure 2. Observed peak S4 per minute is presented row-wise in each columnar panel, which are given in categories of MEO and GSO satellites, respectively, for L1, L2, and L5 for all of the nights. Each peak S4 value is given a unique color in the color bar, corresponding to the occurrence of weak (green, $0.2 < S4 \leq 0.5$), moderate (blue, $0.5 < S4 \leq 0.8$), and strong (red, $S4 > 0.8$) scintillation.

Therefore, considering different occurrence morphologies which have been found to depend upon geometries of satellite constellations (MEO or GSO), the severity of scintillation per night is obtained in terms of total minutes (including all the scintillation-affected IPPs for a signal) of S4 occurrence in categories of the weak ($0.3 < S4 \leq 0.5$), moderate ($0.5 < S4 \leq 0.8$), and strong ($S4 > 0.8$) scintillations. Additionally, a statistical significance of the peak S4 is obtained by taking an average of the S4 values in the top-quartile range for a given night in the next part of the analysis. Outliers are removed by excluding those S4 values which were above the $[Q3 + 1.5 \times (Q3 - Q1)]$, where Q1 and Q3 are levels of respective quartiles. The nights for which the S4 number occurrence is found to be less than 15 in the weak category of scintillations are discarded from the analysis. These results are shown in Figure 3, where bars correspond to those nights when scintillations in different categories have occurred, and the red asterisks show the statistical peak S4 values per night above each bar (right abscissa). Many nights during the equinoctial months show scintillations with significant daily variations in the number of occurrences as well as the peak S4 values. The number of occurrences is found to change drastically on a given night when the scintillations are observed either from MEO or GSO satellites. For example, on L1 (Figure 3a,b), the number occurrence is always found higher on MEO than GSO at any night. This difference is found to be consistent when we note the height of green, blue, or red bars on MEO-L1 versus GSO-L1, respectively. Notably, a very large occurrence of weak scintillations is observed on both the MEO and GSO signals; however, a good number of moderate scintillations are observed on MEO L1 compared to the GSO L1. In particular, a very little occurrence of strong scintillation is seen (mostly in October 2022) on both the MEO and GSO L1, which is observed to increase for MEO L2 and L5 but not

for GSO signals. The higher occurrence of strong scintillations corresponds to a higher statistical average of peak S4 values on those nights. Therefore, the statistical average of peak S4 values provides a higher confidence based on occurrence statistics of the severity of scintillations on a given night. Interestingly, this is also found to follow on those nights when very high weak scintillations are found to occur which correspond to very low peak S4 values.

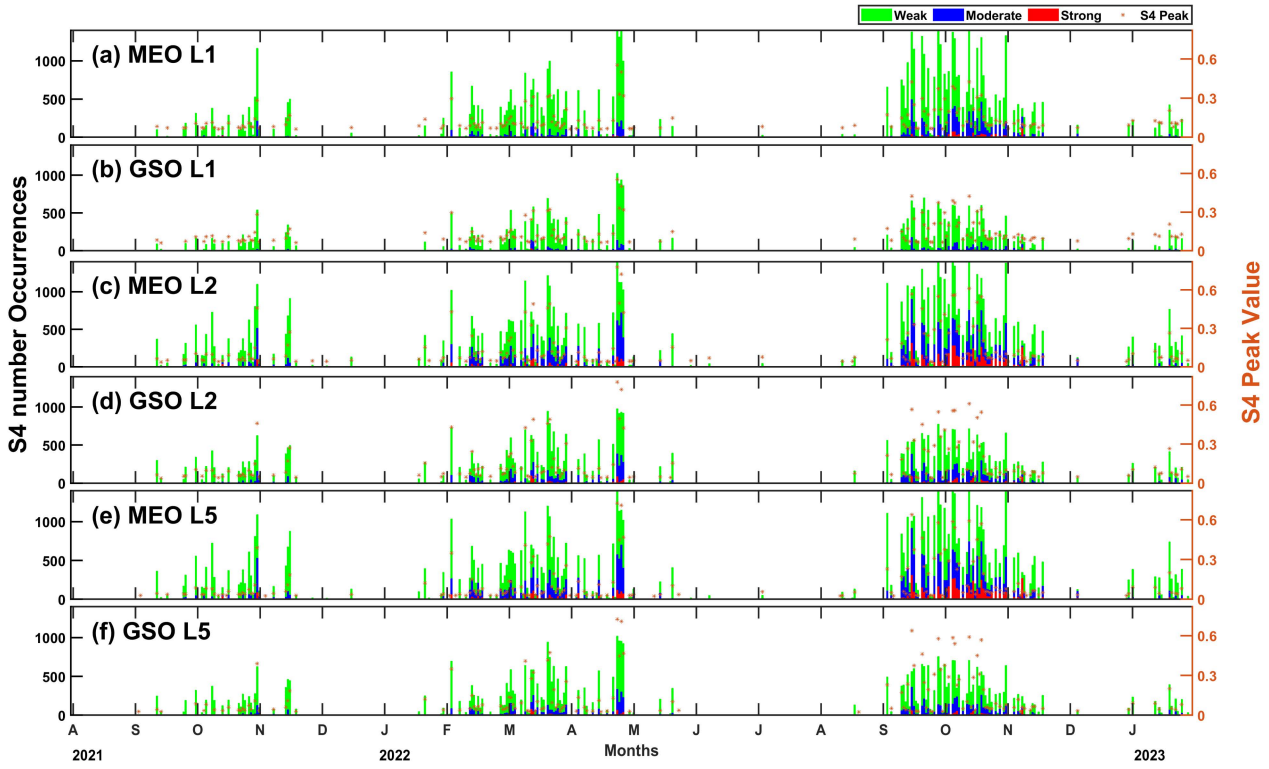

Figure 3. Total S4 occurrences for each night are given in weak (green), moderate (blue), and strong (red) scintillations on the left ordinate axis. Also, the statistically derived average of S4 values from the top-quartile range for each night is shown as an asterisk marker on the right-ordinate axis.

In comparison to L1 (Figure 3a,b), both L2 (Figure 3c,d) and L5 (Figure 3e,f) show a larger number of occurrences of strong and moderate scintillations. However, the weak scintillations show decreasing dependence while decreasing the frequency of the signal. This decrement in the weak scintillations on L1 is found to translate to a higher occurrence of moderate and strong scintillations on L2 and L5, irrespective of MEO or GSO satellites. However, the MEO (Figure 3a,c,e) versus GSO (Figure 3b,d,f) difference remains similar for each of the L2 and L5 as seen on L1 above.

From these figures, the higher (lower) S4 occurrence during the equinox (solstice) is observed in accordance with the previous studies [36,51,52], and what is more, the present study extends the observations to include BeiDou, GALILEO, and QZSS constellations. During the March and September equinoxes of 2022, the severity of scintillations, as observed from all panels of Figure 3 depicts a higher occurrence of S4 (~1000 to 1400 on MEO and ~500 to 800 on GSO signals) for many nights. Such high and continuous daily S4 occurrences need further analysis both in terms of their scientific origin and the difference in severity across MEO and GSO satellites from different constellations.

This particular aspect is further analyzed by focusing on the percentage of satellites which are simultaneously affected, corresponding to S4 > 0.2 for each minute of a particular night. The analysis reveals an interesting scenario every night which differs for different signals (Figure 4) from the MEO and GSO groups of satellites.

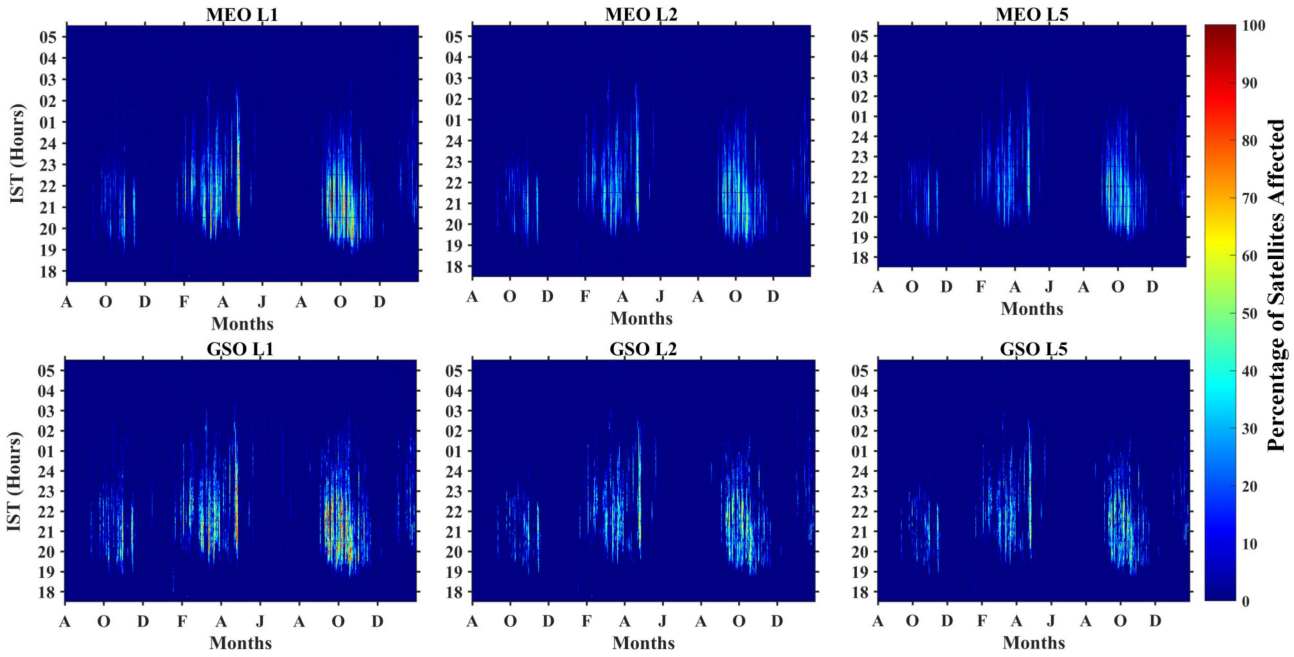

Figure 4. The percentage of scintillation-affected satellites per minute from MEO (upper panel) and GSO satellites (lower panel) are shown, respectively, for L1, L2, and L5 in columnar panels. The color bar represents the percentage of satellites affected at a time (ordinate axis) on a night (abscissa).

Two interesting features are noteworthy from Figure 4, the first one is the slightly higher percentage of satellites affected by scintillation on L1 compared to other signals on both the MEO and GSO satellites. And the second is a very high percentage of affected satellites (above 80%) on some nights with large daily variation. In general, a higher percentage of GSO satellites are found to be affected by scintillation on any night compared to MEO.

The seasonal percentage distribution of scintillation occurrence in terms of weak (green), moderate (blue), and strong (red) intensity for the total observation period is obtained using Equation (3). The results of this analysis are given in Figure 5. For all the MEO and GSO satellites, most of the strong scintillations are observed in the September equinoxes (SE) followed by the March equinox (ME). The summer solstice (SS) mostly shows weak scintillations throughout compared to winter solstices (WS). Abdu et al. [54] and Tsunoda [55] have explained the seasonal occurrence pattern of the EPBs based on the alignment of the solar terminator with the geomagnetic field lines. A closer alignment between the two is found to enhance the eastward electric field during the post-sunset hours, which supports a high growth rate of the Rayleigh–Taylor instability [56,57]. Accordingly, several studies using Radar and GPS observations have shown higher scintillation occurrence during the equinoctial months [37,58,59]. However, our study expands the scintillation observations across all the GNSS constellations categorized in MEO and GSO satellites in this context [36]. From Figure 5, it is evident that irrespective of constellations, the scintillation activity increases with a decrease in the signal frequency. The occurrence percentage of moderate scintillations is found to be higher than strong scintillations, and weak scintillations are found to be the most frequently occurring for all signals of MEO and GSO satellites.

To further this analysis, a complementary cumulative distribution function (CCDF) for each signal is estimated for varying S4 intensities as given in Section 2. Figure 6 shows CCDF results for MEO (left panel) and GSO satellites (right panel) for the respective S4 bins. L2 and L5 signals are found to follow a similar CCDF for the MEO; however, they differ slightly for S4 > 0.2 in the case of GSO. Notably, L1 shows a slower rate of decrement in the probability of both the MEO and GSO cases compared to L2 and L5 signals, but in

the case of GSO, the decrement in CCDF of the L1 signal (blue) mostly remains closer to that of L5 (green). The rapid decrement from an initial high value of CCDF till the first transition in slopes (at S4~0.09 for MEO and S4~0.15 for GSO) has been attributed to non-significant scintillations mostly due to noise [12]. Beyond the first transition, the probability of scintillations is found to decrease slowly and continuously. It is known that the fade patterns change for amplitude scintillations varying from weak to moderate and strong scintillations (Humphreys et al., Sales et al.) [13,46]. This result indicates an overall demarcation of the frequency effect (dispersive nature of ionosphere) on signals and their relationships with the severity of S4 and its occurrence. The inter-frequency relation of amplitude scintillation is obtained by using all the observations with S4 > 0.2 on different signals of MEO and GSO satellites. Figure 7 shows three scatter plots, one each for a possible combination of signals of MEO and GSO for a direct comparison. The first striking feature is the large scatter of MEO signals between L1 versus L2 (Figure 7a) and L5 (Figure 7b), compared to the highly linear response between L2 and L5 (Figure 7c). However, the small spread in the scatter plot for GSO signal combinations is noteworthy. The respective slopes are shown in the equations of the linear LS fit (red lines), which show that the linear fits are weighted towards L2 (Figure 7a,d) and L5 (Figure 7b,e), whereas all the combinations of GSO signals show a very good correlation.

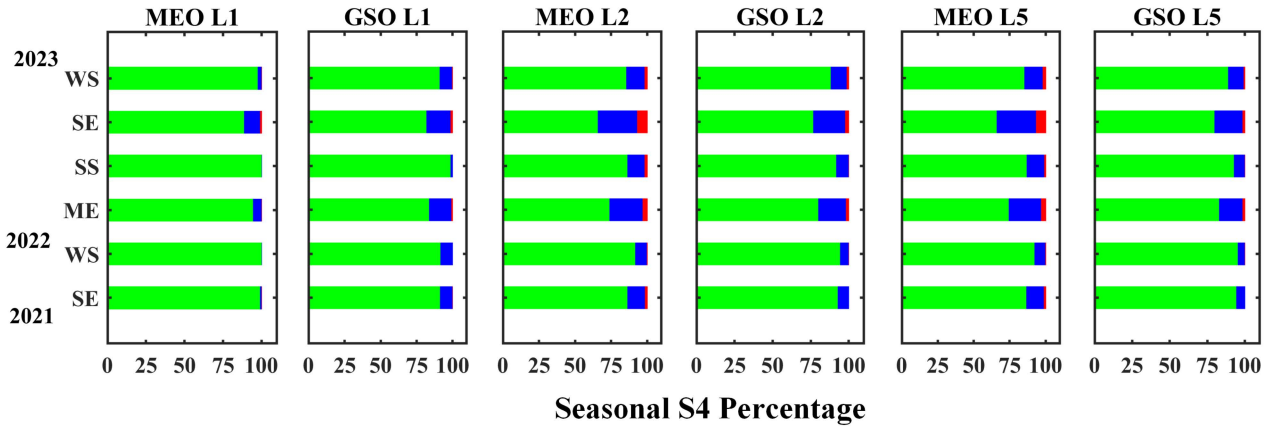

Figure 5. The seasonal percentage S4 distribution is given in terms of intensity (weak-green, moderate-blue, and strong-red,), respectively, for MEO and GSO satellites and their available signals for the seasons during 2021–2023. The seasonal acronyms correspond to SE = September Equinox (August to October); WS = Winter Solstice (November to January); ME = March Equinox (February to April); and SS = Summer Solstice (May to July).

One of the aims of this study is to understand the effect of amplitude scintillations on satellites transmitting L1 (which is a uniform GNSS signal across most of the constellations). Figure 8 shows the percentage of the available satellites per minute affected by scintillations (S4 > 0.2) from MEO (left panel) and GSO (right panel), binned in increments of 10%. The height of each bar represents the total minutes for which the percentage of satellites were affected during August 2021–January 2023. MEO satellites show a continuous decrement in the percentage of affected satellites, resulting in a lesser count of total minutes for which a higher percentage of satellites are affected. However, there are some striking differences when it comes to the GSO group of satellites. The lowest percentage bin (0–10%) is found to be affected by a lower number of minutes for GSO, which increases for the next bin by 10–20%. The number of minutes then decreases successively up to a percentage bin of 50–60%, and thereafter, it shows almost no change in the number of minutes for which satellites are affected by the scintillations. Thus, the MEO and GSO groups of satellites show a matching effect for bins between 10% and 60%, and the effect on GSO majorly differs for high-percentage bins.

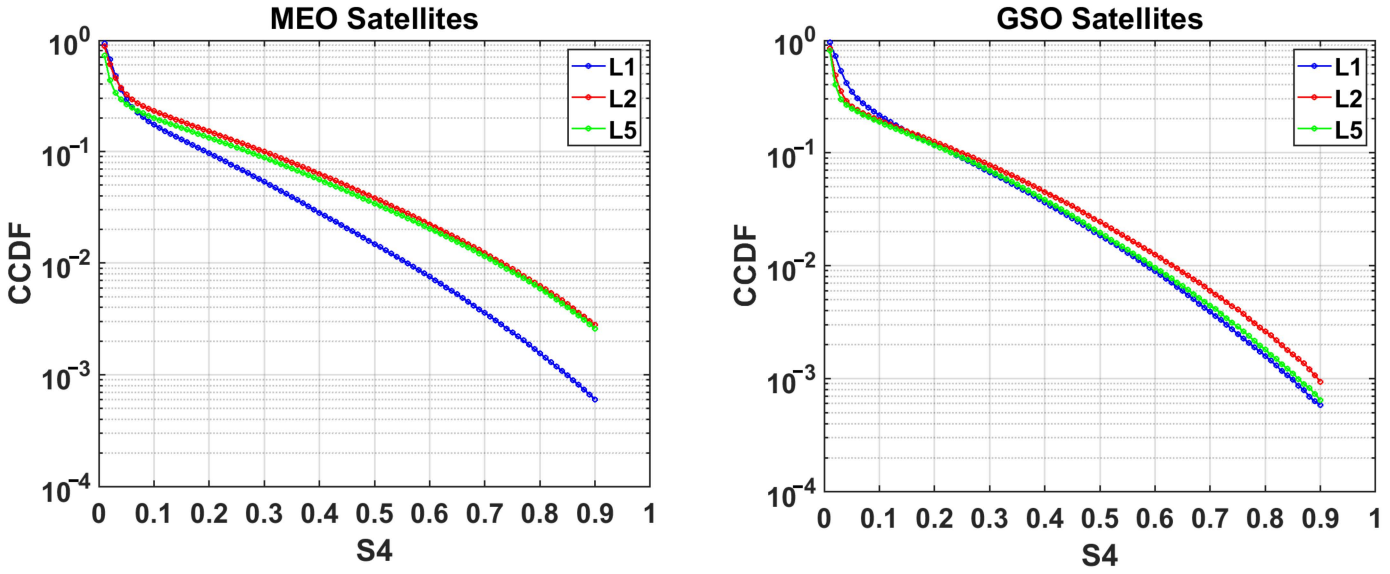

Figure 6. Variations in the complementary cumulative distribution function (CCDF) are shown for L1 (blue), L2 (red), and L5 (green) across all the intensities of the S4 binned in 0.01 increments, respectively, for MEO and GSO satellites. Total S4 > 0 occurrence for MEO = 2,788,999 and GSO = 869,275.

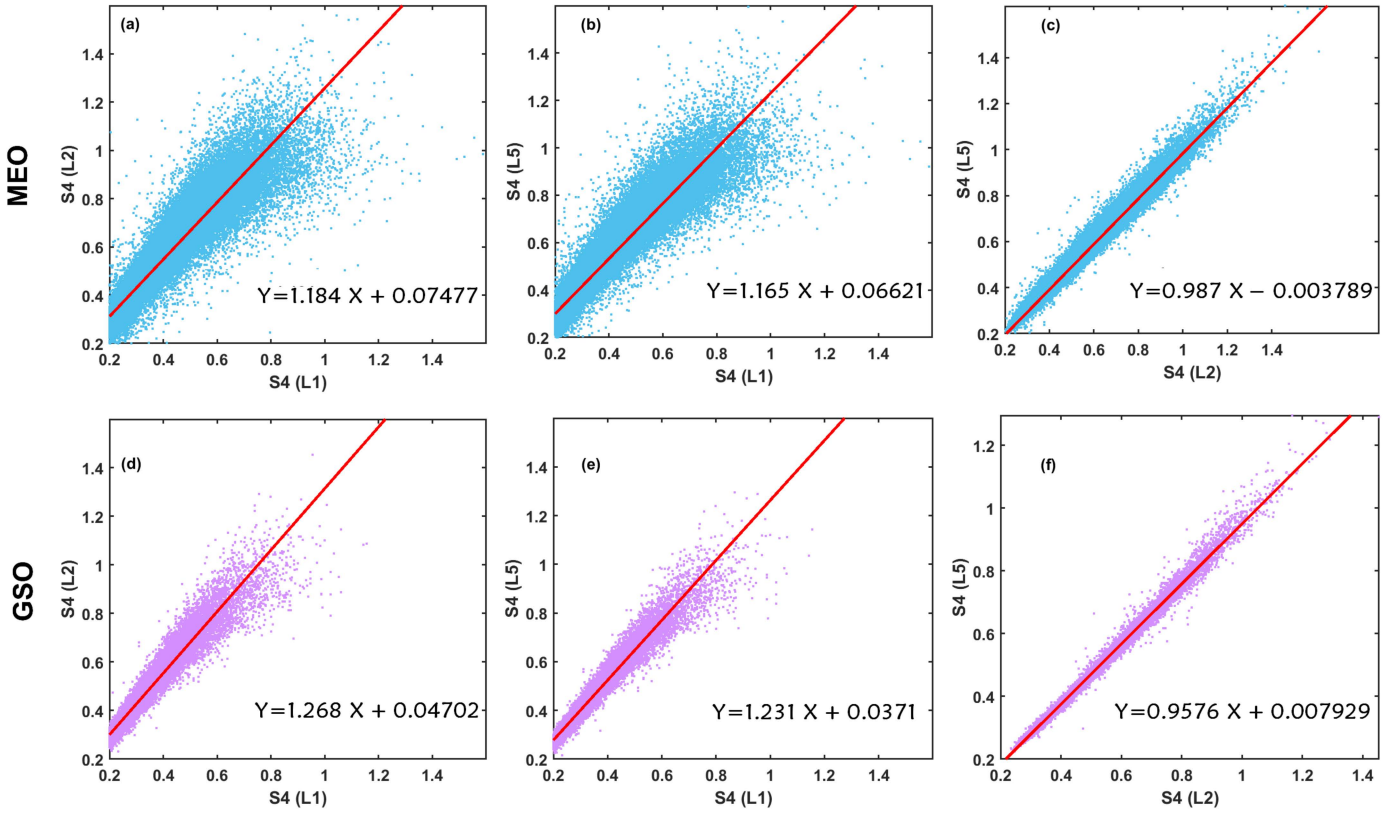

Figure 7. Comparative distribution of occurrence of S4 > 0.2 on different signals (**a**,**d**) L1 and L2 (**b**,**e**) L1 and L5 and (**c**,**f**) L2 and L5, respectively, given for MEO (upper panels) and GSO (lower panels) satellites. A linear fit is shown by the red line and the respective fit equation is given in each panel in form of $Y = mX + c$, where m represent slope of the fit.

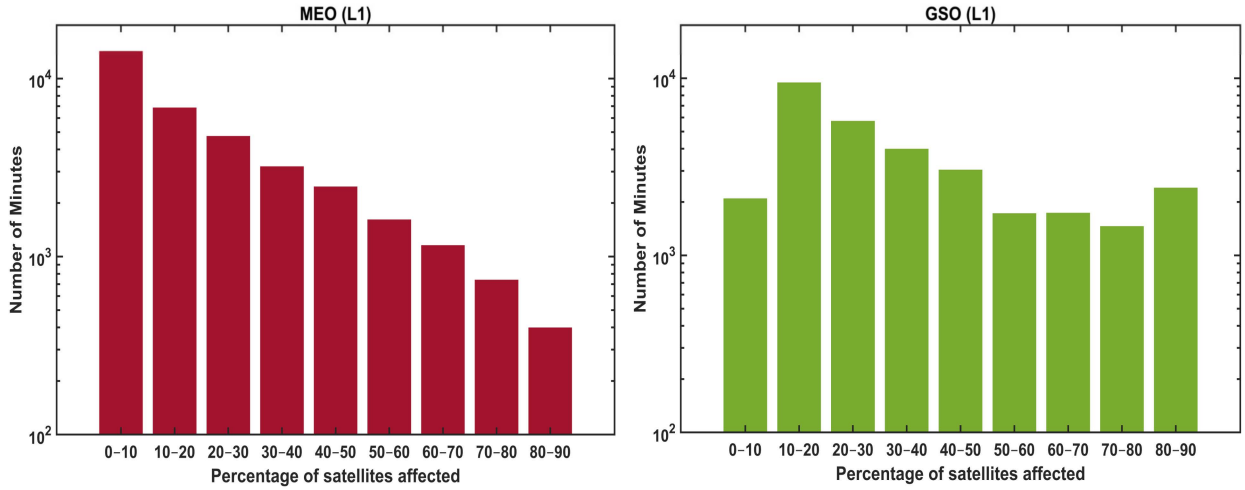

Figure 8. Percentage of satellites affected by scintillation (S4 > 0.2) for the number of minutes (log10 scale) is shown for MEO (left panel) and GSO (right panel) L1 with a bin increment of 10%.

4. Discussion

Most of the previous results on GNSS scintillations were based on either a GPS or multi-constellation comparison with a few case studies of geostationary satellite signals, like SBAS [19,34,50,51]. A comprehensive inspection of the results presented in this study shows that the overall statistics of scintillation occurrence and the frequency dependence of the severity of scintillations are found to match well with the previous studies. However, since this is possibly the first study to compare the scintillations from MEO and GSO groups of satellites, a few aspects have emerged which are worth emphasizing in the context of the present understanding.

The scintillation occurrence given in Figure 3 shows different patterns with overall lower rates on GSO signals than MEO. Since the number of satellites available during each night determines the scintillation occurrence rate for a group of satellites [11,36], it is possible to observe higher S4 occurrence on MEO. Slower relative motion between the MEO satellite link and zonally drifting equatorial plasma bubbles could be one of the possible geometrical reasons behind such an occurrence. It is known that the irregularities drift at an average eastward velocity in a range of about 70–150 m/s [49] during pre-midnight hours and more than one bubble can pass over a low-latitude station in this duration [60]. So, the faster-moving MEO satellite links could cut across multiple bubbles in different geometries for the same duration, resulting in a higher number of scintillation links compared to rather stable or slow-moving GSO links. And, of course, the higher number of MEO satellites compared to GSO could directly affect the total S4 occurrence for a given signal transmission (i.e., L1). The IPPs corresponding to the SBAS, NavIC, and other geostationary satellites are shown in Figure 1, which validates the closeness of multiple satellite links in the GSO group at the KLEF location. This aspect needs further investigation because we also note that multiple closely spaced GSO satellites can decrease the space diversity for scintillations considering varying width and spacing between EPBs on a given night [42]. One of the possible causes behind this result could be the percentage of satellites which are simultaneously affected each minute (see Figure 4).

In this context, it is pertinent to emphasize the space-diversity mitigation effects which are related to the angular distance between two geostationary satellites [42] when observed from a low latitude station. They have shown that amplitude scintillations over GSO links are also affected by the width and spacing of the EPBs and the latitude of the station. Thus, the higher percentage of GSO satellites affected by scintillation could be possible due to the present geometry of GSO signals as seen from the KLEF station (see Figure 1). Moraes et al. [61] have studied scintillation characteristics from two SBAS satellites observed from two low latitude stations using the L1 signal. Our results on

GSO-L1 mostly match their results. A recent study by Sousasantos et al. [50] shows that the occurrence of strong scintillations depends upon the degree of alignment between the propagation path and the EPBs. The higher percentage of affected satellites on L1 signal compared to that on L2 and L5 signals could be possible because more satellites transmit the L1 signal [2]. Also, most of the higher percentage is found to occur during post-sunset to midnight irrespective of MEO or GSO satellites/signals which is a well-known aspect. Thus, the dynamics of the EPBs are found to affect different signals differently which causes variations in the number of affected satellites. This analysis thus establishes that during the peak hours of scintillations at low latitude stations like KLEF, most of the available satellites above the 30° elevation angle may be affected by the scintillations. It is known that the scintillations can lead to a higher probability of LoL in low latitudes [2], and this can result in sudden changes in the satellite geometry and dilution of precision [7,62]. Recently, Yousuf et al. [3] have shown that the LoL events on GPS L1 can directly control the kinematic precise point positioning in low latitudes showing night-to-night, seasonal, and even long-term ionospheric impact on the positioning.

Further, the CCDF analysis has provided an insight into the probability of scintillations. The probability of MEO scintillations with S4 > 0.3 as well as all other bins are found to match well with the CCDF results of Costa et al. [42]; Sales et al. [12]; and Moraes et al. [61], as observed from low-latitude stations elsewhere around the globe. However, in the case of GSO satellites, it is found that the L1 and L5 links exhibit a similar slope in CCDF (Figure 6). As noted in the context of Figures 1 and 4 above, it is once again emphasized here that the closely spaced geostationary satellite links can be simultaneously affected by the zonal width of EPBs and spacing between consecutive EPBS on a given night [48,58]. Thus, in the context of the present results on CCDF of GSO satellite links, a similar probability of severe scintillations on L5 and L1 links can be explained through the space-diversity mitigation effect.

Another non-identical result for GSO satellites compared to MEO is found in context to the correlation of S4 occurrences among the L1, L2, and L5. Results from different equatorial and low latitude locations (South American sector) from Salles et al. [12] using the GPS constellation have shown that a non-linear relationship exists between S4 values over the GPS-L1 versus GPS-L2 or GPS-L5. Our study also confirms the non-linearity (mostly for MEO signals) with high scatter; however, we find that the S4 shows rather higher slopes and lesser scatter (better correlation) among GSO signals. Thus, the scintillation models may use this relationship (Figure 7) for the GSO group of satellites for improvement in the forecast of S4 occurrence on other frequencies.

It is interesting to note that the number of minutes for which the percentage of satellites are affected by scintillations shows a matching effect between MEO and GSO for less than ~60%. It is intriguing partly due to an almost equal number of minutes for which the percentage stands to be equal over different bins. This possibly indicates that the ratio of the affected to the available satellites remains consistent in both the MEO and GSO groups. Considering about 35–40 available satellites per minute from MEO and 9–12 from GSO, such consistency was unexpected. We understand that this could occur due to the spatially homogeneous distribution of scintillations (S4 > 0.2) within the geometrical cone defined by 30–90° elevation over the KLEF site. This assumption may not be valid for most of the local times and nights. Therefore, we consider the difference in the number of affected minutes between MEO and GSO above 60% bins. It is known that the closely spaced geostationary satellite links can be simultaneously affected when the signal passes through the same EPB at about the 350–400 km altitude region. Costa et al. [42] have also found that the spacing between the successive EPBs also plays a major role in affecting the GSO links, which can continue to observe scintillations simultaneously as the equatorial plasma bubbles pass over the site, which is in contrast to the fast-moving MEO links.

Our study has addressed this aspect through a new scenario of comparative MEO versus GSO satellites and underscored the need for further detailed investigations on the occurrence of scintillation and its severity and distribution of satellite availability

in different constellations. Such an analysis shall also support developing a mitigation algorithm using multi-GNSS constellations to avoid extreme GNSS black-out scenarios.

5. Conclusions

This study investigates the post-sunset irregularities in the ionosphere in terms of amplitude scintillation measured S4 index from a multi-constellation and multi-frequency GNSS receiver installed at a low latitude Indian location KLEF, Guntur, just below the equatorial ionization anomaly crest zone. A robust comparative analysis of scintillations obtained from the two groups of MEO and GSO satellites over all three signals is performed. This comparative analysis revealed that along with the well-known solar activity control of scintillation occurrence and seasonal and local time dependence (all from the literature), the geometry of the line-of-sight of the signal, the number of available satellites and the frequency of the signal also play crucial roles in the occurrence and strength of the scintillations. In a nutshell, this study highlights the following:

i. The observed pattern of scintillations from the geostationary and geosynchronous satellites (called GSO) is found to be different from the other medium Earth-orbiting GNSS satellites (called MEO) in terms of a lesser temporal extent on a given night. Furthermore, moderate and strong scintillations (i.e., overall S4 > 0.5) are observed on a greater number of nights with higher occurrence from the MEO group of GNSS satellites. Similarly, the statistically derived peak S4 for a night is found to be weighted by the number of occurrences of scintillations of different intensities (i.e., weak, moderate, or strong). This implies confidence in the peak S4 to represent the scintillation scenario of a night.
ii. The number of occurrences of scintillations is found to be always higher for MEO than GSO for any category of scintillations. The occurrence of strong and moderate scintillation is found to be higher on L2 and L5 for both the MEO and GSO groups, where the occurrence of weak scintillations is found to be highest on all of the signals. The statistical average of peak S4 values on a given night is found to provide higher confidence on the occurrence of the severity of scintillations.
iii. The percentage occurrence of scintillation-affected satellites is found to be higher on L1 compared to other signals, wherein a contrasting higher percentage of affected satellites over GSO than MEO is observed. This could possibly be due to the higher number of MEO satellites transmitting L1 as a standard navigation signal. The faster movement of MEO links compared to GSO links can also enhance the possibility of a higher occurrence of scintillations from the multiple drifting plasma bubbles. However, it shall also be noted that the higher number of closely spaced GSO satellites could also produce similar results owing to lesser space diversity which needs further investigation. Thus, the number of satellites transmitting a particular signal and the angular spacing and elevation angle also play a crucial role in the percentage occurrence pattern.
iv. The complementary probability (CCDF) of S4 occurrence shows a lesser occurrence of more severe scintillations with different variations among signals of MEO and GSO satellites. While a clear demarcation between the L2/L5 signals and L1 is found over the MEO, in case of GSO, the CCDF over L5 is found to match mostly with the L1 signal. This could possibly originate from the space diversity gain effect known to impact the closely spaced geostationary satellite links. However, the scintillation relationship between L1 and the other two signals is found to be weighted towards lower frequencies (with higher slopes and lesser scatter on GSO signals).
v. The analysis of the percentage of satellites affected on L1 shows a close match between MEO and GSO for the total number of minutes in each 10% bin up to 60%. But the number of minutes for which the percentage of affected satellites remains larger than 60% is found to be higher for GSO. This result indicates homogeneous spatial patterns in the scintillation distribution over a low latitude site, which could originate from

closely spaced GSO links and highlight the role of the number of available satellites with the geometry of the links, being the deciding factor.

These results emphasize the effect of scintillation on various constellations which are now distributed either in MEO or GSO orbits and their transmission frequencies under changing ionospheric conditions. It is known that the scintillations in the equatorial and low latitudes are affected by solar and geomagnetic activity, seasons, local time, lower atmospheric perturbations reaching the ionosphere, and different ionospheric anomalies. So, it is emphasized that the background solar activity needs to be comparable while attributing the scintillation occurrence from two different sites. The scintillations in the L-band radio frequencies are responsible for random amplitude and phase fluctuations which at times can lead to the LoL on the signal in the receiver [2,4–6]. At present, different types of GNSS receivers use different software and hardware techniques that enable them to distinctively adapt to a variety of scintillation effects. So, different receivers exhibit diverse impacts on the signals due to scintillations in terms of LoL and other impacts on a user position estimate. Hence, a multi-constellation and multi-frequency analysis at any location for a longer period using multiple types of receivers could provide a better understanding of the effect of scintillation on satellite-based navigation and could help in identifying the best set of satellites and constellations to implement mitigation strategies for accurate position solutions. We could establish some prominent features of scintillation occurrence when the same signal is transmitted from different orbits, leading to a varying geometric link traversing through the equatorial ionospheric irregularities. In the future, we aim to study the scintillation and LoL scenarios during extreme events using multiple receivers with varying solar activity. Knowing that a combination of two or more GNSS constellations can result in more available satellites, this can result in a suitable distribution of IPPs such that the non-scintillating signals are still available for determination of positioning. It could help to develop the inter GNSS models for precise point position solutions where higher accuracy will be obtained with continuity and availability of the signals.

Author Contributions: Conceptualization, N.D.; methodology, N.D. and S.K.P.; software, R.V. and J.R.K.K.D.; validation, N.D., S.K.P. and J.R.K.K.D.; formal analysis, N.D., J.R.K.K.D., S.K.P. and R.V.; investigation, N.D., S.K.P. and R.V.; resources, N.D. and S.K.P.; data curation, N.D. and S.K.P.; writing—original draft preparation, R.V. and S.K.P.; writing—review and editing, N.D. and S.K.P.; visualization, N.D., J.R.K.K.D., R.V. and S.K.P.; supervision, N.D. and S.K.P.; project administration, S.K.P.; funding acquisition, S.K.P. All authors have read and agreed to the published version of the manuscript.

Funding: The present work has been carried out under the Core Research Grant (CRG) project sponsored by the Science & Engineering Research Board (SERB) (A statutory body of the Department of Science & Technology, Government of India) New Delhi, India, vide File No: CRG/2019/003394.

Data Availability Statement: The multi-constellation and multi-frequency GNSS scintillation data are obtained from the Septentrio PolaRx5S GNSS receiver established at the study location.

Acknowledgments: R.K.V. is extremely thankful to the Director, NARL, Department of Space, Government of India, for providing the necessary facilities and supporting visits to carry out part of this work at NARL under the collaborative research program.

Conflicts of Interest: The authors declare no conflicts of interest. The funders had no role in the design of the study; in the collection, analyses, or interpretation of data; or in the writing of the manuscript.

References

1. Yeh, K.C.; Liu, C.-H. Radio Wave Scintillations in the Ionosphere. *Proc. IEEE* **1982**, *70*, 324–360. [CrossRef]
2. Srinivasu, V.K.D.; Dashora, N.; Prasad, D.S.V.V.D.; Niranjan, K. Loss of Lock on GNSS Signals and Its Association with Ionospheric Irregularities Observed over Indian Low Latitudes. *GPS Solut.* **2022**, *26*, 34. [CrossRef]
3. Yousuf, M.; Dashora, N.; Sridhar, M.; Dutta, G. Long-Term Impact of Ionospheric Scintillations on Kinematic Precise Point Positioning: Seasonal and Solar Activity Dependence over Indian Low Latitudes. *GPS Solut.* **2022**, *27*, 40. [CrossRef]
4. Damaceno, J.G.; Bolmgren, K.; Bruno, J.; De Franceschi, G.; Mitchell, C.; Cafaro, M. GPS Loss of Lock Statistics over Brazil during the 24th Solar Cycle. *Adv. Space Res.* **2020**, *66*, 219–225. [CrossRef]

5. Pezzopane, M.; Pignalberi, A.; Coco, I.; Consolini, G.; De Michelis, P.; Giannattasio, F.; Marcucci, M.F.; Tozzi, R. Occurrence of GPS Loss of Lock Based on a Swarm Half-Solar Cycle Dataset and Its Relation to the Background Ionosphere. *Remote Sens.* **2021**, *13*, 2209. [CrossRef]
6. De Michelis, P.; Consolini, G.; Pignalberi, A.; Lovati, G.; Pezzopane, M.; Tozzi, R.; Giannattasio, F.; Coco, I.; Marcucci, M.F. Ionospheric Turbulence: A Challenge for GPS Loss of Lock Understanding. *Space Weather* **2022**, *20*, e2022SW003129. [CrossRef]
7. Hofmann-Wellenhof, B.; Lichtenegger, H.; Wasle, E. (Eds.) Satellite Signals. In *GNSS—Global Navigation Satellite Systems: GPS, GLONASS, Galileo, and More*; Springer Vienna: Vienna, Austria, 2008; pp. 55–104. ISBN 978-3-211-73017-1.
8. Aarons, J. The Role of the Ring Current in the Generation or Inhibition of Equatorial F Layer Irregularities during Magnetic Storms. *Radio Sci.* **1991**, *26*, 1131–1149. [CrossRef]
9. Basu, S.; Kudeki, E.; Basu, S.; Valladares, C.E.; Weber, E.J.; Zengingonul, H.P.; Bhattacharyya, S.; Sheehan, R.; Meriwether, J.W.; Biondi, M.A.; et al. Scintillations, Plasma Drifts, and Neutral Winds in the Equatorial Ionosphere after Sunset. *J. Geophys. Res. Space Phys.* **1996**, *101*, 26795–26809. [CrossRef]
10. Shanmugam, S.; Jones, J.; MacAulay, A.; Van Dierendonck, A.J. Evolution to Modernized GNSS Ionoshperic Scintillation and TEC Monitoring. In Proceedings of the 2012 IEEE/ION Position, Location and Navigation Symposium, Myrtle Beach, SC, USA, 23–26 April 2012; pp. 265–273.
11. Hlubek, N.; Berdermann, J.; Wilken, V.; Gewies, S.; Jakowski, N.; Wassaie, M.; Damtie, B. Scintillations of the GPS, GLONASS, and Galileo Signals at Equatorial Latitude. *J. Space Weather Space Clim.* **2014**, *4*, A22. [CrossRef]
12. Salles, L.A.; Vani, B.C.; Moraes, A.; Costa, E.; de Paula, E.R. Investigating Ionospheric Scintillation Effects on Multifrequency GPS Signals. *Surv. Geophys.* **2021**, *42*, 999–1025. [CrossRef]
13. Salles, L.A.; Moraes, A.; Vani, B.; Sousasantos, J.; Affonso, B.J.; Monico, J.F.G. A Deep Fading Assessment of the Modernized L2C and L5 Signals for Low-Latitude Regions. *GPS Solut.* **2021**, *25*, 122. [CrossRef]
14. De Oliveira Moraes, A.; da Silveira Rodrigues, F.; Perrella, W.J.; de Paula, E.R. Analysis of the Characteristics of Low-Latitude GPS Amplitude Scintillation Measured During Solar Maximum Conditions and Implications for Receiver Performance. *Surv. Geophys.* **2012**, *33*, 1107–1131. [CrossRef]
15. Guo, K.; Zhao, Y.; Liu, Y.; Wang, J.; Zhang, C.; Zhu, Y. Study of Ionospheric Scintillation Characteristics in Australia with GNSS during 2011–2015. *Adv. Space Res.* **2017**, *59*, 2909–2922. [CrossRef]
16. Jiao, Y.; Xu, D.; Morton, Y.; Rino, C. Equatorial Scintillation Amplitude Fading Characteristics Across the GPS Frequency Bands. *Navigation* **2016**, *63*, 267–281. [CrossRef]
17. Delay, S.H.; Carrano, C.S.; Groves, K.M.; Doherty, P.H. A Statistical Analysis of GPS L1, L2, and L5 Tracking Performance during Ionospheric Scintillation. In Proceedings of the 2015 ION Pacific PNT Conference, Honolulu, HI, USA, 20–23 April 2015; pp. 1–9.
18. Carrano, C.; Groves, K.; McNeil, W.J.; Doherty, P.H. Scintillation Characteristics Across the GPS Frequency Band. In Proceedings of the 25th International Technical Meeting of the Satellite Division of the Institute of Navigation 2012, ION GNSS 2012, Nashville, TN, USA, 17–21 September 2012; Volume 3, pp. 1972–1989.
19. De Oliveira Moraes, A.; Costa, E.; Abdu, M.A.; Rodrigues, F.S.; de Paula, E.R.; Oliveira, K.; Perrella, W.J. The Variability of Low-Latitude Ionospheric Amplitude and Phase Scintillation Detected by a Triple-Frequency GPS Receiver. *Radio Sci.* **2017**, *52*, 439–460. [CrossRef]
20. Moraes, d.O.A.; Vani, B.C.; Costa, E.; Sousasantos, J.; Abdu, M.A.; Rodrigues, F.; Gladek, Y.C.; de Oliveira, C.B.A.; Monico, J.F.G. Ionospheric Scintillation Fading Coefficients for the GPS L1, L2, and L5 Frequencies. *Radio Sci.* **2018**, *53*, 1165–1174. [CrossRef]
21. Akala, A.O.; Awoyele, A.; Doherty, P.H. Statistics of GNSS Amplitude Scintillation Occurrences over Dakar, Senegal, at Varying Elevation Angles during the Maximum Phase of Solar Cycle 24. *Space Weather* **2016**, *14*, 233–246. [CrossRef]
22. Ghafoori, F.; Skone, S. Impact of Equatorial Ionospheric Irregularities on GNSS Receivers Using Real and Synthetic Scintillation Signals. *Radio Sci.* **2015**, *50*, 294–317. [CrossRef]
23. Otsuka, Y.; Shiokawa, K.; Ogawa, T. Equatorial Ionospheric Scintillations and Zonal Irregularity Drifts Observed with Closely-Spaced GPS Receivers in Indonesia. *J. Meteorol. Soc. Japan. Ser. II* **2006**, *84*, 343–351. [CrossRef]
24. Valladares, C.E.; Villalobos, J.; Sheehan, R.; Hagan, M.P. Latitudinal Extension of Low-Latitude Scintillations Measured with a Network of GPS Receivers. *Ann. Geophys.* **2004**, *22*, 3155–3175. [CrossRef]
25. Dashora, N.; Pandey, R. Observations in Equatorial Anomaly Region of Total Electron Content Enhancements and Depletions. *Ann. Geophys.* **2005**, *23*, 2449–2456. [CrossRef]
26. Kelley, M.C. *The Earth's Ionosphere: Plasma Physics and Electrodynamics*; Academic Press: Cambridge, MA, USA, 2009; ISBN 0-08-091657-0.
27. Rino, C. *The Theory of Scintillation with Applications in Remote Sensing*; Wiley-IEEE Press: Hoboken, NJ, USA, 2011; ISBN 978-0-470-64477-5.
28. Rino, C.; Breitsch, B.; Morton, Y.; Jiao, Y.; Xu, D.; Carrano, C. A Compact Multi-Frequency GNSS Scintillation Model. *Navigation* **2018**, *65*, 563–569. [CrossRef]
29. Kelley, M.C.; Makela, J.J.; Paxton, L.J.; Kamalabadi, F.; Comberiate, J.M.; Kil, H. The First Coordinated Ground- and Space-Based Optical Observations of Equatorial Plasma Bubbles. *Geophys. Res. Lett.* **2003**, *30*, 1766. [CrossRef]
30. Ledvina, B.M.; Makela, J.J. First Observations of SBAS/WAAS Scintillations: Using Collocated Scintillation Measurements and All-Sky Images to Study Equatorial Plasma Bubbles. *Geophys. Res. Lett.* **2005**, *32*. [CrossRef]

31. Carrano, C.S.; Rino, C.L. A Theory of Scintillation for Two-Component Power Law Irregularity Spectra: Overview and Numerical Results. *Radio Sci.* **2016**, *51*, 789–813. [CrossRef]
32. Bhattacharyya, A.; Kakad, B.; Gurram, P.; Sripathi, S.; Sunda, S. Development of Intermediate-Scale Structure at Different Altitudes within an Equatorial Plasma Bubble: Implications for L-Band Scintillations. *J. Geophys. Res. Space Phys.* **2017**, *122*, 1015–1030. [CrossRef]
33. DasGupta, A.; Ray, S.; Paul, A.; Banerjee, P.; Bose, A. Errors in Position-Fixing by GPS in an Environment of Strong Equatorial Scintillations in the Indian Zone. *Radio Sci.* **2004**, *39*, 1–8. [CrossRef]
34. Goswami, S.; Paul, K.S.; Paul, A. Assessment of GPS Multifrequency Signal Characteristics during Periods of Ionospheric Scintillations from an Anomaly Crest Location. *Radio Sci.* **2017**, *52*, 1214–1222. [CrossRef]
35. Rama Rao, P.; Gopi Krishna, S.; Niranjan, K.; Prasad, D. *Study of Spatial and Temporal Characteristics of L-Band Scintillations over the Indian Low-Latitude Region and Their Possible Effects on GPS Navigation*; Copernicus GmbH: Göttingen, Germany, 2006; Volume 24, pp. 1567–1580.
36. Srinivasu, V.K.D.; Dashora, N.; Prasad, D.S.V.V.D.; Niranjan, K.; Krishna, S.G. On the Occurrence and Strength of Multi-Frequency Multi-GNSS Ionospheric Scintillations in Indian Sector during Declining Phase of Solar Cycle 24. *Adv. Space Res.* **2018**, *61*, 1761–1775. [CrossRef]
37. Sripathi, S.; Sreekumar, S.; Banola, S. Characteristics of Equatorial and Low-Latitude Plasma Irregularities as Investigated Using a Meridional Chain of Radio Experiments Over India. *J. Geophys. Res. Space Phys.* **2018**, *123*, 4364–4380. [CrossRef]
38. Paul, A.; Sur, D.; Haralambous, H. Multi-Wavelength Coordinated Observations of Ionospheric Irregularity Structures from an Anomaly Crest Location during Unusual Solar Minimum of the 24th Cycle. *Adv. Space Res.* **2020**, *65*, 1402–1413. [CrossRef]
39. Singh, S.B.; Rathore, V.S.; Singh, A.K.; Singh, A.K. Ionospheric Irregularities at Low Latitude Using VHF Scintillations during Extreme Low Solar Activity Period (2008–2010). *Acta Geod. Geophys.* **2017**, *52*, 35–51. [CrossRef]
40. Engavale, B. Spatial Correlation Function of Intensity Variations in the Ground Scintillation Pattern Produced by Equatorial Spread-F Irregularities. *Indian J. Radio Space Phys.* **2005**, *34*, 22–32.
41. Biswas, T.; Paul, A. Signal-In-Space Performance Under Multiconstellation Environment From an Indian Low Latitude Station. *Radio Sci.* **2021**, *56*, e2020RS007119. [CrossRef]
42. Costa, E.; Roddy, P.A.; Ballenthin, J.O. Space Diversity Mitigation Effects on Ionospheric Amplitude Scintillation with Basis on the Analysis of C/NOFS Planar Langmuir Probe Data. *Radio Sci.* **2020**, *55*, 1–11. [CrossRef]
43. Yeh, W.-H.; Lin, C.-Y.; Liu, J.-Y.; Chen, S.-P.; Hsiao, T.-Y.; Huang, C.-Y. Superposition Property of the Ionospheric Scintillation S4 Index. *IEEE Geosci. Remote Sens. Lett.* **2020**, *17*, 597–600. [CrossRef]
44. Van Dierendonck, A.J. Ionospheric Scintillation Monitoring Using Commercial Single Frequency C/A Code Receivers. In Proceedings of the ION GPS 93, Salt Lake City, UT, USA, 22–24 September 1993.
45. Secan, J.A.; Bussey, R.M.; Fremouw, E.J.; Basu, S. An Improved Model of Equatorial Scintillation. *Radio Sci.* **1995**, *30*, 607–617. [CrossRef]
46. Humphreys, T.E.; Psiaki, M.L.; Kintner, P.M. Modeling the Effects of Ionospheric Scintillation on GPS Carrier Phase Tracking. *IEEE Trans. Aerosp. Electron. Syst.* **2010**, *46*, 1624–1637. [CrossRef]
47. Humphreys, T.E.; Psiaki, M.L.; Ledvina, B.M.; Cerruti, A.P.; Kintner, P.M. Data-Driven Testbed for Evaluating GPS Carrier Tracking Loops in Ionospheric Scintillation. *IEEE Trans. Aerosp. Electron. Syst.* **2010**, *46*, 1609–1623. [CrossRef]
48. Vilà-Valls, J.; Linty, N.; Closas, P.; Dovis, F.; Curran, J.T. Curran Survey on Signal Processing for GNSS under Ionospheric Scintillation: Detection, Monitoring, and Mitigation. *Navigation* **2020**, *67*, 511. [CrossRef]
49. Sethi, H.S.; Dashora, N. Automated Power Spectrum Analysis of Low-Latitude Ionospheric Scintillations Recorded Using Software GNSS Receiver. *GPS Solut.* **2020**, *24*, 33. [CrossRef]
50. Sousasantos, J.; Affonso, B.J.; Moraes, A.; Rodrigues, F.S.; Abdu, M.A.; Salles, L.A.; Vani, B.C. Amplitude Scintillation Severity and Fading Profiles Under Alignment Between GPS Propagation Paths and Equatorial Plasma Bubbles. *Space Weather* **2022**, *20*, e2022SW003243. [CrossRef]
51. Muella, M.T.A.H.; de Paula, E.R.; Kantor, I.J.; Rezende, L.F.C.; Smorigo, P.F. Occurrence and Zonal Drifts of Small-Scale Ionospheric Irregularities over an Equatorial Station during Solar Maximum—Magnetic Quiet and Disturbed Conditions. *Adv. Space Res.* **2009**, *43*, 1957–1973. [CrossRef]
52. Abadi, P.; Saito, S.; Srigutomo, W. Low-Latitude Scintillation Occurrences around the Equatorial Anomaly Crest over Indonesia. *Ann. Geophys.* **2014**, *32*, 7–17. [CrossRef]
53. Kintner, P.M.; Ledvina, B.M.; de Paula, E.R.; Kantor, I.J. Size, Shape, Orientation, Speed, and Duration of GPS Equatorial Anomaly Scintillations. *Radio Sci.* **2004**, *39*, 1–23. [CrossRef]
54. Abdu, M.A.; Bittencourt, J.A.; Batista, I.S. Magnetic Declination Control of the Equatorial F Region Dynamo Electric Field Development and Spread F. *J. Geophys. Res. Space Phys.* **1981**, *86*, 11443–11446. [CrossRef]
55. Tsunoda, R.T. Control of the Seasonal and Longitudinal Occurrence of Equatorial Scintillations by the Longitudinal Gradient in Integrated E Region Pedersen Conductivity. *J. Geophys. Res. Space Phys.* **1985**, *90*, 447–456. [CrossRef]
56. Woodman, R.F.; La Hoz, C. Radar Observations of F Region Equatorial Irregularities. *J. Geophys. Res. (1896–1977)* **1976**, *81*, 5447–5466. [CrossRef]
57. Farley, D.T.; Bonelli, E.; Fejer, B.G.; Larsen, M.F. The Prereversal Enhancement of the Zonal Electric Field in the Equatorial Ionosphere. *J. Geophys. Res. Space Phys.* **1986**, *91*, 13723–13728. [CrossRef]

58. Hysell, D.L.; Burcham, J.D. JULIA Radar Studies of Equatorial Spread F. *J. Geophys. Res. Space Phys.* **1998**, *103*, 29155–29167. [CrossRef]
59. Joshi, L.M. Equatorial F-region Irregularities during Low and High Solar Activity Conditions. *Indian J. Radio Space Phys.* **2012**, *41*, 208.
60. Das, S.K.; Patra, A.K.; Kherani, E.A.; Chaitanya, P.P.; Niranjan, K. Relationship Between Presunset Wave Structures and Interbubble Spacing: The Seeding Perspective of Equatorial Plasma Bubble. *J. Geophys. Res. Space Phys.* **2020**, *125*, e2020JA028122. [CrossRef]
61. Moraes, A.; Sousasantos, J.; Costa, E.; Pereira, B.A.; Rodrigues, F.; Galera Monico, J.F. Characterization of Scintillation Events With Basis on L1 Transmissions From Geostationary SBAS Satellites. *Space Weather* **2024**, *22*, e2023SW003656. [CrossRef]
62. Aboelmagd, N.; Karamat, T.B.; Jacques, G. *Fundamentals of Inertial Navigation, Satellite-Based Positioning and Their Integration*; Springer: Berlin/Heidelberg, Germany, 2013. [CrossRef]